Key Engineering Materials
ISSN: 1662-9795, Vol. 926, pp 1762-1769
doi:10.4028/p-l23f52

Submitted: 2022-01-21
Revised: 2022-02-02
Accepted: 2022-02-03
Online: 2022-07-22

Influence of the Laser Welding Direction of Thin DP600 and the Residual Stresses Relaxation Obtained by Simulation and Neutron Diffraction

Miaoran LIU[1,2,a], Afia KOUADRI-HENNI[1,2,b*] and Benoit MALARD[3,c]

[1]INSA Rennes, 20 avenue des Buttes de Coësmes, 35708, Rennes, France

[2]ROMAS Team, Laboratory of Digital Sciences of Nantes (LS2N), UMR CNRS 6004, 1 rue de la Noë, 44300, Nantes, France

[3]CIRIMAT, Université de Toulouse, CNRS, INPT, UPS, 4 Allée Emilie Monso 31030 Toulouse, France

[a]miaoranliu@foxmail.com, [b]afia.kouadri-henni@insa-rennes.fr, [c]benoit.malard@ensiacet.fr

*Corresponding Author: afia.kouadri-henni@insa-rennes.fr

Keywords: DP600 steel, residual stresses, neutron diffraction, cyclic tensile

Abstract. Laser-welded structures are often subjected to dynamic service loads ranging from cyclic fluctuations to completely random ones. The laser-welded lap joints suffer from defects resulting in notch effects, surface cracks, residual strains and stresses. The fatigue strength of the laser-welded lap joints is reduced significantly because of the presence of these defects, and the size of the welded joints is small. Therefore, the mechanical strength of laser-welded structures must be defined in terms of the fatigue strength and residual stress of the obtained joints or assemblies. To analyze the above-discussed effects, this paper proposed two approaches: numerical and experimental methods. The originality of the work is to weld the rolled sheet in three directions (0°, 45°, 90°). The residual stresses before and after low cyclic tensile tests of assemblies obtained from overlapped thin DP600 steel sheets were calculated by ABAQUS. The obtained results were compared to the experimental data by neutron diffraction. The presented results in terms of residual stresses curves, spatial distributions of residual stresses obtained at the end of laser welding and low-cycle fatigue. It showed the relaxation effect of residual stresses and the direction effect of welding. These results have been explained by several factors.

Introduction

In the automotive industry, lightweight and safety are very important problems. Selecting high-quality materials and advanced manufacturing techniques, and using safe and reliable detection methods can effectively solve the above problems. In general, dual-phase steel is one of the most important materials to make the automobile lightweight. In this process, the laser welding technology can not only improve the efficiency but also reduce the heat-affected zone and increase the depth-to-width ratio of the welds. Therefore, laser welding technology has been widely used in the automobile industry [1]. Based on existing research, it can be found that due to the high content of alloying elements in dual-phase steel, it is easy to deform and produce residual stresses and strains under the action of thermal. In practice, the automobile will experience different dynamic service loads. In this case, the superposition of residual stresses and external loads reduces the mechanical properties and accuracy, producing fatigue cracks and other defects, and even fatigue fractures [2]. And for almost all materials, the rolling process can cause anisotropy of the material. Therefore, it is necessary to accurately measure the distribution of laser welding residual stress in different rolling directions (0°, 45°, 90°) and fatigue residual stress after cyclic loads, analyze the relationships between them, and take necessary measures to improve the safety of the automobile driving process.

With the development of finite element technology, finite element software has shown great potential. ABAQUS is commonly applied with the advantage of obtaining the residual stress field and adding the residual stress field in subsequent calculations [3].

This paper aims at studying the laser welding residual stress for the DP600 dual-phase steel welded structures taking into account rolling directions, and the relaxation of residual stress after low-cycle

fatigue. Specifically, a fully coupled thermo-mechanical finite element analysis and an elastic-plastic material constitutive model were used to calculate the laser welding residual stress and strain by emulating the welding process. During the process of subsequent low-cycle fatigue residual stress, the obtained results were employed as a predefined stress field. Furthermore, the residual stress with different rolling directions and relaxation of the welded structure was investigated. The simulation results were validated by the experimental results.

Experiments by Neutron Diffraction

The proposed experiments aim to evaluate the residual stresses (on the upper surface of the weld beads in longitudinal and transverse directions) by neutron diffraction in the ferritic phase of the plates after laser welding and low-cycle fatigue. This paper realized the measurements in three directions (0°, 45°, 90°). The parameters of laser welding are shown in Table 1.

Table 1 Parameters of laser welding for the sample

Laser Power [kW]	Welding Speed [m/min]	Defocus [mm]	Gap [mm]
4	3	-0.33	0.1

A gauge volume of 1x1x5 mm^3 was defined with the 5 mm aperture along the axis of the weld (to improve intensity), when possible (i.e. for longitudinal and transverse measurements only). This paper realized the scan through the welded zones: base metal, heat-affected zone and fusion zone on the mid-plate in the longitudinal and transverse directions. The results were compared to simulation data. In the first approach, residual stresses were calculated from the measured strains applying Hooke's law (Eq.1) in the principal direction approximation:

$$\sigma_{\mathrm{i}} = \frac{\mathrm{E}_{110}}{1+\mathrm{v}_{110}}\left[\varepsilon_{\mathrm{i}} + \frac{\mathrm{v}_{110}}{1-2v_{110}}\sum\varepsilon_j\right] \tag{1}$$

where i, j presents longitudinal and transverse, with the following values of Young modulus (E110 =220 GPa) and Poisson's ratio (0.33). Because the normal stress at the surface of the plate is null, this paper applied the following formula for each measurement point, to obtain the Bragg angle corresponding to the stress-free q0, 110:

$$2\theta_0 = 2\cdot\sin^{-1}\left(\frac{(1+\nu)\cdot\sin\theta_{\mathrm{normal}}\cdot\sin\theta_{\mathrm{axial}}\cdot\sin\theta_{\mathrm{transverse}}}{(1-\nu)\cdot\sin\theta_{\mathrm{axial}}\cdot\sin\theta_{\mathrm{transverse}}+\nu\cdot\sin\theta_{\mathrm{normal}}\cdot(\sin\theta_{\mathrm{axial}}+\sin\theta_{\mathrm{transverse}})}\right) \tag{2}$$

Simulations of Laser Welding Residual Stress

Laser welding residual stress was evaluated through the use of a fully coupled thermo-mechanical approach. It began with thermal analysis and elastic-plastic mechanical analysis simultaneously. After heating and subsequent cooling processes, laser welding residual stresses were finally calculated.

Finite element model. The finite element model and the mesh are shown in Fig.1. The thickness of the base metal is 1.25 mm, with a 0.1 mm gap between the two base metals. Laser lap welding was used in this paper.

There were 8144 elements in total for the model and element type, the C3D8T mesh in the ABAQUS was employed to calculate the laser welding residual stress. Both convection and radiation were applied as thermal boundary conditions to the surface of the model. And the thermal load was a conical heat source with Gaussian distribution using the DFLUX subroutine in ABAQUS.

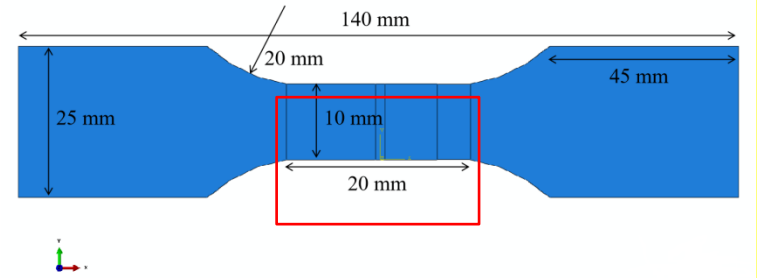

a

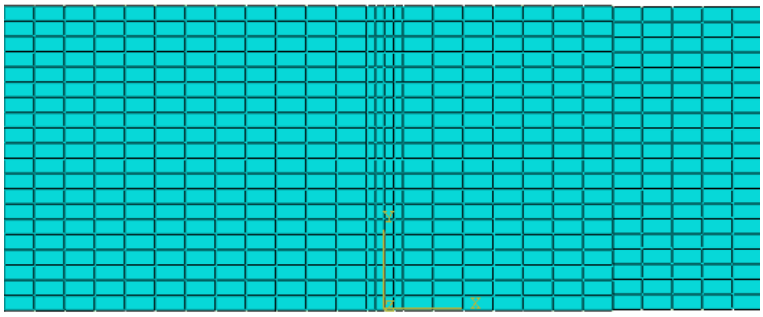

b

Fig.1 Finite element model and mesh (a Finite element model, b Mesh of the red frame)

Material constitutive model. The constitutive relationship of material reflects the law of stress changing with strain under a certain deformation, which is the foundation for the study of material strength and life.

The most commonly used constitutive models are the Ludwik Model and the Voce Model. The Ludwik Model is used to study the flow behavior of martensite in DP600 dual-phase steel, while the Voce Model is focused on ferrite. Using the two models separately will cause errors in the simulation results, therefore, two models were combined in this paper [4].

$$\sigma = \omega \times \sigma_{Ludwik} + (1-\omega) \times \sigma_{Voce} \tag{3}$$

where ω is the proportion of martensite, the value of ω equals 0.4. According to the experimental results, the constitutive model is as follows:

$$\sigma = 0.4 \times (380 - 4784.28\varepsilon^{1215.12}) + 0.6 \times \{380 + 607.50 \times [1 - \exp(-24.53\varepsilon)]\} \tag{4}$$

Anisotropy method. The rolling direction and the welding direction are shown in Fig.2. The angle between the two directions is the rolling angle θ. When the welding direction is parallel to the rolling direction, the rolling angle is 0°. When the welding direction is perpendicular to the rolling direction, the rolling angle is 90°. In this paper, the rolling angles of 0°, 45° and 90° were simulated.

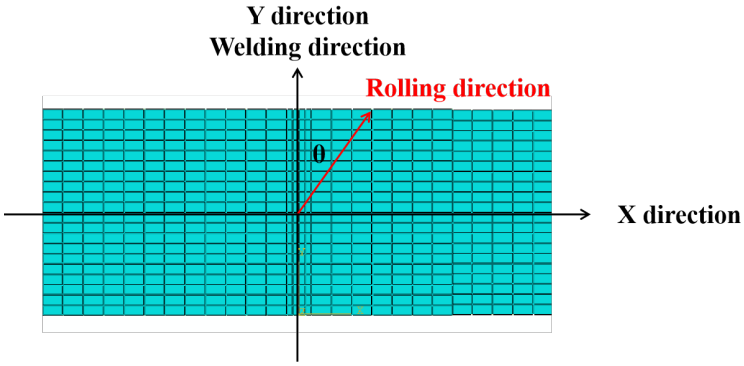

Fig.2 Rolling direction and welding direction

For almost all materials, rolling leads to the anisotropy of the material. The large deformation during the rolling process results in different plastic behavior of DP600 dual-phase steel in different directions. The influence of anisotropy on the plastic flow behavior of DP600 dual-phase steel depends on its mechanical properties [5]. Many theories can be applied to describe the anisotropy of the material, the most common of which is the Hill48 yield criterion with six parameters [6].

The Hill48 yield criterion is the extension of the Von Mises yield criterion, which can be expressed as follows [7]:

$$\mathrm{f} = \sqrt{F(\sigma_{22}-\sigma_{33})^2 + G(\sigma_{33}-\sigma_{11})^2 + H(\sigma_{11}-\sigma_{22})^2 + 2L\sigma_{23}^{\ 2} + 2M\sigma_{31}^{\ 2} + 2N\sigma_{12}^{\ 2}} \tag{5}$$

where f is the effective stress and defines the plastic flow. F, G, H, L, M and N are constants obtained by tests of the material in different directions.

The anisotropy of DP600 was taken into account in the simulation in three directions (0°, 45°, 90°). The results showed that the residual stress varies with the different rolling directions.

Simulations of Low-Cycle Fatigue Residual Stress

In the low-cycle fatigue residual stress simulation, the same finite element mesh model was utilized as an alternative to element type C3D8R. In addition, the laser welding residual stress calculated by the previous analysis was set as the predefined stress field. The boundary conditions were changed to ENCASTRE and ZSYMM. The cycle period time was 0.2 s, the circular frequency was 10π, the load was a sine wave stress with the amplitude of 300 MPa, the stress ratio of 0, and the frequency of 5 Hz. Subsequently, investigations on the relaxation of the residual stress were shown. It is worth noting that the comparison with the experimental results will validate the simulation results more sufficiently [8].

Results and Discussions

Fig.3 shows the longitudinal and transverse laser welding residual stress curves with different rolling directions by simulation and experiment of S11 and S22. S11 means the normal stress in X direction in ABAQUS. S22 means the normal stress in Y direction in ABAQUS.

As seen in Fig.3a and b, the laser welding residual stress is related to anisotropy, different rolling direction influences the magnitude of residual stress. In the longitudinal direction, the residual stress increases with the increase of the rolling angle. In the transverse direction, as the rolling angle increases, the residual stress in the zone away from the weld decreases, while the residual stress in the weld and heat-affected zone increases.

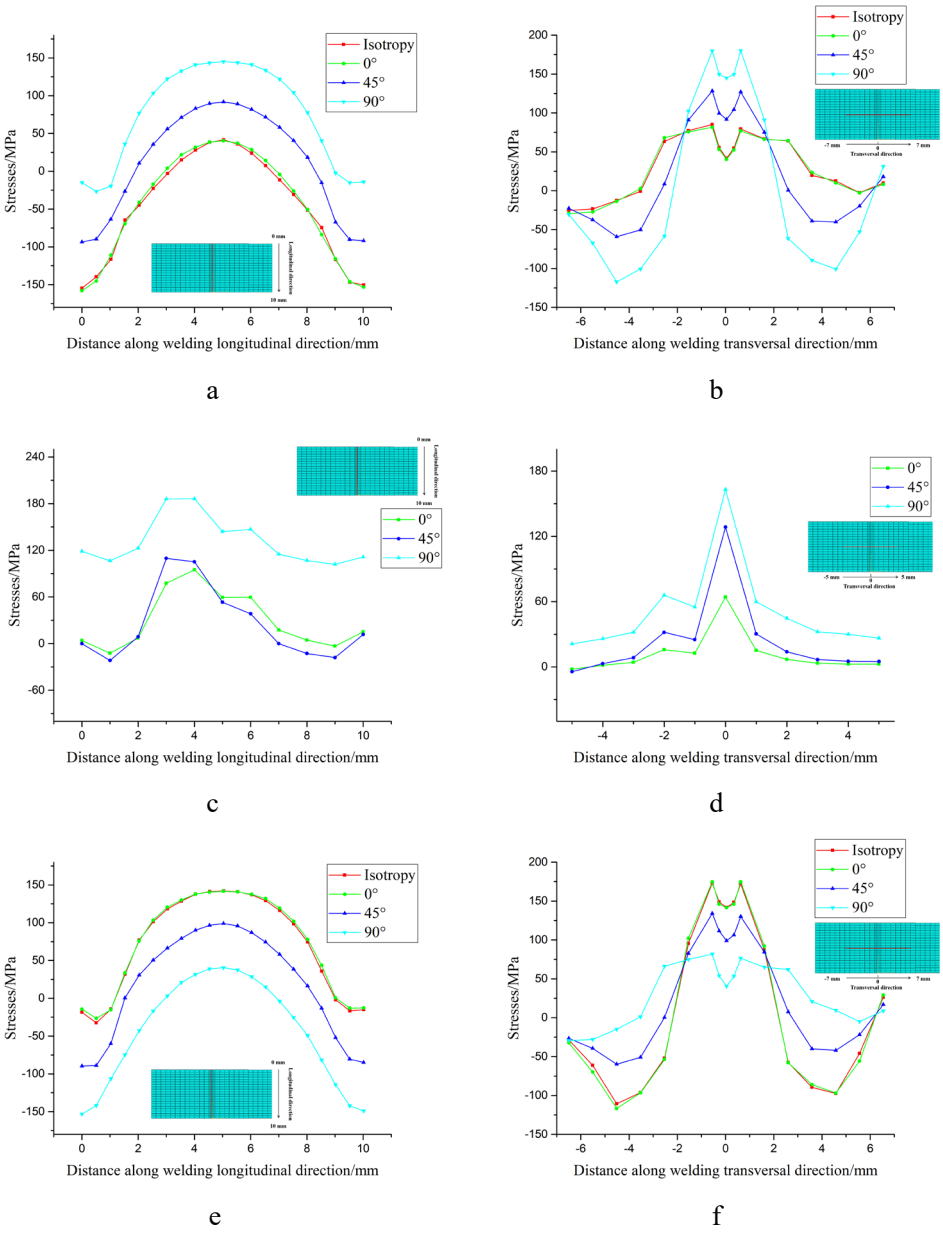

Fig.3 Laser welding residual stress with different rolling directions (a longitudinal residual stress by simulation of S11, b transverse residual stress by simulation of S11, c longitudinal residual stress by experiment of S11, d transverse residual stress by experiment of S11, e longitudinal residual stress by simulation of S22, f transverse residual stress by simulation of S22)

Fig.3c and d shows the results obtained by the experiment with the same parameters as the simulation. As can be seen from the figure, with the increase of the rolling angle, the distribution of the longitudinal residual stress is similar to the simulation, but the distribution of the transverse residual stress is different in the area away from the weld. This is because the distribution of laser welding residual stress is influenced by many factors. In the simulation, the boundary condition is the absolute rigid constraint, and the molten pool fluidity is ignored. The flow of the molten pool in the experiment has a significant effect on the distribution of residual stress. And the processing technology of the DP600 plates used in the experiment is also one of the reasons for the difference between the results.

And as can be seen in Fig.3e and f, with the rolling angle changes from 0° to 90°, the change rule of S22 is exactly opposite to that of S11, increasing one while decreasing the other. However, regardless of S11 or S22, when the material is assumed to be isotropic, the residual stress is similar to that at the rolling angle of 0°, further verifying the correlation between residual stress and anisotropy.

Meanwhile, no matter which rolling direction is simulated, the maximum value of residual stress is near the center of the weld. This is because when the heat source acts on a certain point of the weld during laser welding, it will cause the material to expand due to the thermal and form an area of compressive stress, and the compressive stress is higher than the yield strength of the material at this temperature so that the material produces compressive plastic deformation. When the heat source continues moving, the material at this point will gradually cool down and the yield strength of the material will gradually increase, thus resulting in high tensile residual stress.

Fig.4 shows the longitudinal and transverse low-cycle fatigue residual stress curves with different rolling directions by simulation and experiment of S11 and S22.

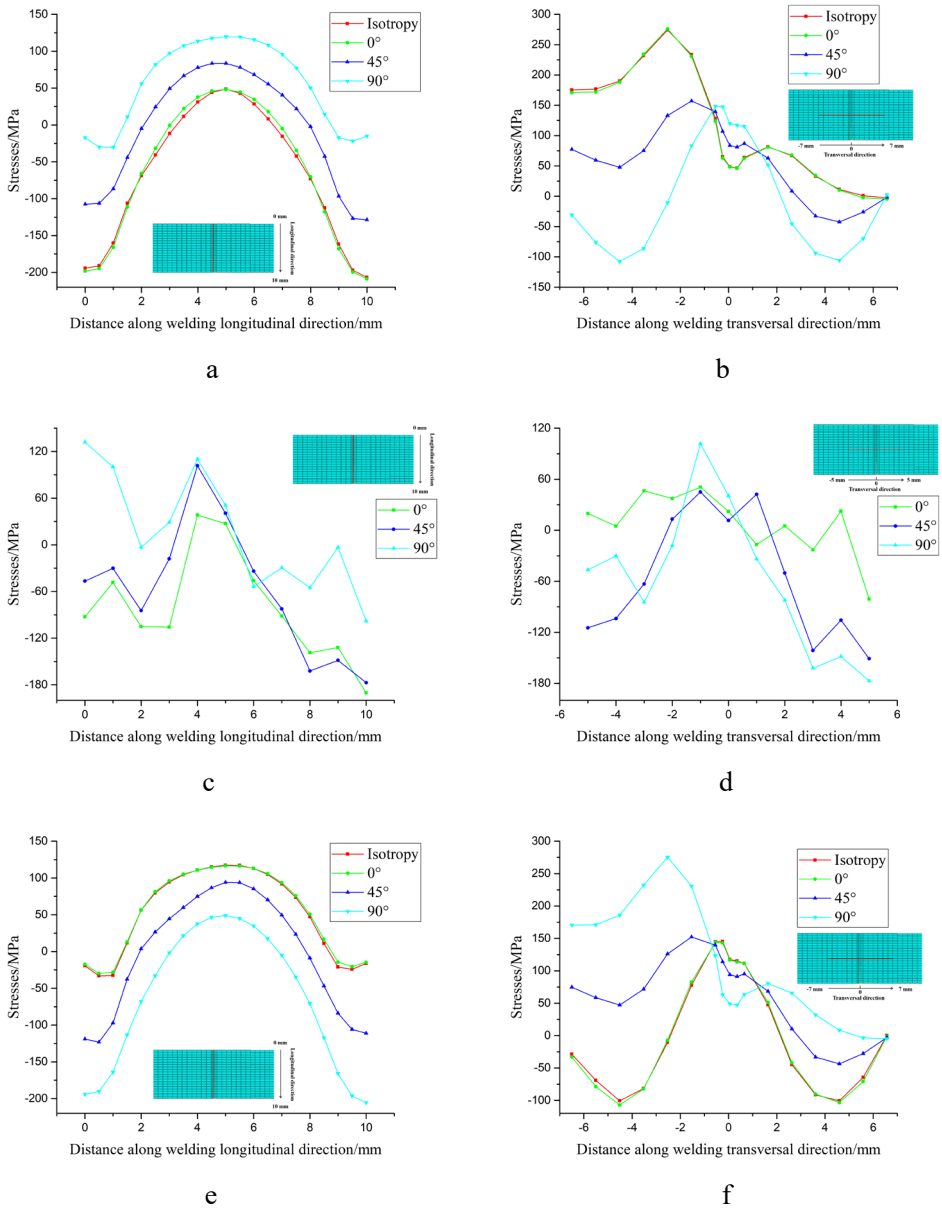

Fig.4 Low-cycle fatigue residual stress with different rolling directions (a longitudinal residual stress by simulation of S11, b transverse residual stress by simulation of S11, c longitudinal residual stress by experiment of S11, d transverse residual stress by experiment of S11, e longitudinal residual stress by simulation of S22, f transverse residual stress by simulation of S22)

It can be seen from Fig.4b and f that because the left end is fixed and the right end is subjected to cyclic loads during the simulation, the mid-planes of the two base metals are not in a straight line. Under external loads, the welded structure is subjected to torque around the weld. So the distribution of low-cycle fatigue transverse residual stress in welded structures is asymmetric.

From Fig.4b, with the increase in rolling angle, the low-cycle fatigue residual stress changes from tensile residual stress to compressive residual stress. During the rolling process, the grains deform along the rolling direction. Because of the texture formation, when the cyclic direction is parallel to the rolling direction, the Schmid factor is larger, which contributes to the grain slip and the plastic deformation, leading to compressive residual stress and increasing the fatigue properties of the material. However, when the direction of the cyclic load is perpendicular to the rolling direction, the Schmid factor is smaller, and the plastic deformation takes place only when the external force is larger, resulting in tensile residual stress and reducing the fatigue properties of the material. And S22 is also opposite to S11.

Fig.4c and d is the results obtained by the experiment. It shows that with the increase of the rolling angle, the distribution of the residual stress no matter longitudinal or transverse is similar to the simulation. Although the magnitude of the residual stress has some differences, more accurate results can be obtained by optimizing the process parameters in the later research.

And the change rule of low-cycle fatigue residual stress with rolling direction is the same as that of laser welding residual stress. It further shows that the magnitude of laser welding residual stress will influence the low-cycle fatigue residual stress.

Fig.5 shows longitudinal and transverse laser welding residual stress and low-cycle fatigue residual stress (Von Mises) by simulation. Von Mises means the Mises equivalent stress in ABAQUS.

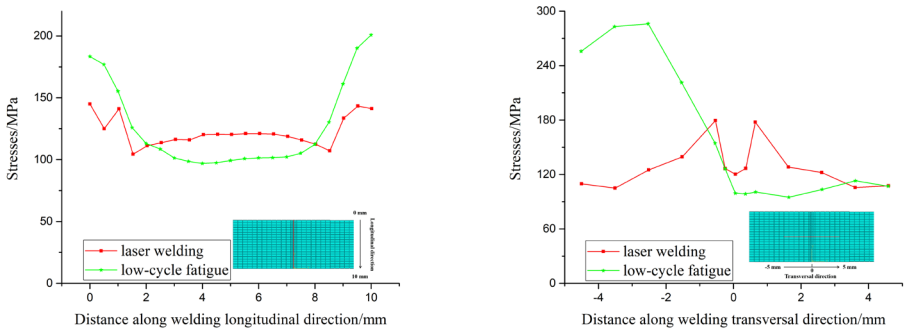

a b

Fig.5 Longitudinal and transverse laser welding residual stress and low-cycle fatigue residual stress by simulation of Von Mises

From Fig.5, it can be seen that after the low-cycle fatigue simulation, the residual stress of the welded structure is redistributed, and local attenuation occurs in the center of the weld and the heat-affected zone. This is because the right end of the welded structure is loaded with cyclic stress. When the applied stress superimposes with the residual stress. The stress in the local area of the welded structure will reach or be higher than the yield strength, and plastic deformation will occur in the local area. Even in some cases, the stress does not reach the yield strength, but the applied stress causes local dislocation of the welded structure. The dislocation must overcome its internal resistance first, and then the crystal slips, causing plastic deformation inside the crystal. When the cyclic stress at the right end is removed, the welded structure will undergo secondary deformation, plastic deformation releases the original deformation of the welded structure, so the residual stress is redistributed and locally attenuated [9].

Conclusions

The following conclusions can be obtained from simulations and experiments of the residual stress after laser welding and low-cycle fatigue of the DP600 dual-phase steel welded structures:

(1) The laser welding residual stress is related to anisotropy, different rolling direction influences the magnitude of residual stress. For S11, in the longitudinal direction, the residual stress increases with the increase of the rolling angle. In the transverse direction, as the rolling angle increases, the residual stress in the zone away from the weld decreases, while the residual stress in the weld and heat-affected zone increases. With the rolling angle changes from 0° to 90°, the change rule of S22 is

exactly opposite to that of S11, increasing one while decreasing the other. No matter which rolling direction is simulated, the maximum value of residual stress is near the center of the weld.

(2) The distribution of low-cycle fatigue transverse residual stress is asymmetric because of the applied cyclic loads. With the increase in rolling angle, the low-cycle fatigue residual stress (S11) changes from tensile residual stress to compressive residual stress. And S22 is also opposite to S11.

(3) The change rule of low-cycle fatigue residual stress with rolling direction is the same as that of laser welding residual stress. The magnitude of laser welding residual stress will influence the low-cycle fatigue residual stress.

(4) Compare the simulation results with the experiment results under the same parameters. With the increase of the rolling angle, the distribution of the laser welding longitudinal residual stress is similar to the simulation, but the distribution of the laser welding transverse residual stress is different in the area away from the weld. Although the magnitude of the low-cycle fatigue residual stress has some differences, the distribution is similar. More accurate results can be obtained by optimizing the process parameters in the later research.

(5) The residual stress of the welded structure is redistributed after the low-cycle fatigue simulation, and local attenuation occurs in the center of the weld and the heat-affected zone.

Acknowledgements

The work was financially supported by China Scholarship Council and the laboratory LS2N of INSA de Rennes.

References

[1] L. Chuan, Z. Jianxun, N. Jing, Numerical and experimental analysis of residual stresses in full-penetration laser beam welding of Ti6Al4V alloy, Rare Metal Mat. Eng. 38 (2009) 1317-1320.

[2] H. Huang, S. Tsutsumi, J. Wang, L. Li, H. Murakawa, High performance computation of residual stress and distortion in laser welded 301L stainless sheets, Finite Elem. Anal. Des. 135 (2017) 1-10.

[3] X. Wang, Q. Meng, W. Hu, Numerical analysis of low cycle fatigue for welded joints considering welding residual stress and plastic damage under combined bending and local compressive loads, Fatigue Fract. Eng. Mater. Struct. 43 (2020) 1064-1080.

[4] S. Liu, Numerical and experimental study on residual stresses in laser beam welding of dual phase DP600 steel plates. Mechanical engineering, Rennes, INSA, 2017.

[5] R. Padmanabhan, A.J. Baptista, M.C. Oliveira, L.F. Menezes, Effect of anisotropy on the deep-drawing of mild steel and dual-phase steel tailor-welded blanks, J. Mater. Process. Technol. 184 (2007) 288-293.

[6] F. Ozturk, S. Toros, S. Kilic, Effects of anisotropic yield functions on prediction of forming limit diagrams of DP600 advanced high strength steel, Procedia Eng. 81 (2014) 760-765.

[7] S. Liu, A. Kouadri-Henni, A. Gavrus, Numerical simulation and experimental investigation on the residual stresses in a laser beam welded dual phase DP600 steel plate: Thermo-mechanical material plasticity model, Int. J. Mech. Sci. 122 (2017) 235-243.

[8] X. Wang, Q. Meng, W. Hu, Fatigue life prediction for butt-welded joints considering weld-induced residual stresses and initial damage, relaxation of residual stress, and elasto-plastic fatigue damage, Fatigue Fract. Eng. Mater. Struct. 42 (2019) 1373-1386.

[9] D. Benasciutti, L. Moro, J. Srnec Novak, Metal plasticity and fatigue at high temperature, Metals, 10 (2020) 326.